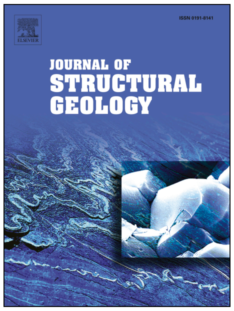

Cataclasis and silt smear on normal faults in weakly lithified turbidites

A. Nicol, C. Childs

PII: S0191-8141(18)30279-7

DOI: 10.1016/j.jsg.2018.06.017

Reference: SG 3688

To appear in: *Journal of Structural Geology*

Received Date: 17 November 2017

Revised Date: 28 May 2018

Accepted Date: 19 June 2018

Please cite this article as: Nicol, A., Childs, C., Cataclasis and silt smear on normal faults in weakly lithified turbidites, *Journal of Structural Geology* (2018), doi: 10.1016/j.jsg.2018.06.017.

Cataclasis and silt smear on normal faults in weakly lithified turbidites

A. Nicol[1*] & C. Childs[2]

[1]GNS Science, PO Box 30368, Lower Hutt, New Zealand
[2]Fault Analysis Group and iCRAG (Irish Centre for Research in Applied Geosciences), UCD School of Earth Sciences, University College Dublin, Belfield, Dublin, Ireland
*Present address: Department of Geological Sciences, University of Canterbury, Private Bag 4800, Christchurch, New Zealand

Abstract

Fault-seal analysis in sand-shale multilayers emphasises the role of shale smear without explicitly accounting for cataclasis. These processes produce low-permeability fault rock and are examined here for small displacement (0.001 to 70 m) normal faults displacing weakly lithified turbidites comprising ~55-80% lithic grains. Late Miocene Mount Messenger Formation (MMF) turbidites from the North Island of New Zealand provide fault rock data over a range of scales from individual grains (~0.1-350 µm) to the height of coastal cliffs (~10-20 m). Fault rock and unfaulted source beds has been analysed using thin sections, SEM images, particle-size distribution (PSD) measurements and outcrops of faults mainly in cross section. Cataclasis associated with particle size and macroscopic porosity reduction of protolith sandstones commences at low fault shear strains (<1) and continues as fault displacement accrues. The relationship between particle-size reduction and displacement is non-linear with initial rapid cataclasis facilitated by disaggregation of weak lithic and altered feldspar grains along pre-existing grain defects (e.g., grain boundaries, fractures and altered cleavage planes). Silt smear, by contrast, is not accompanied by significant particle-size reduction and appears to have been achieved by intergrain slip and micro-faulting. Despite the occurrence of silt smear, cataclasis can produce a significant proportion (>50%) of the total fault-rock in sand-silt multilayers. The resulting fault-rock thickness varies by up to three orders of magnitude for a given fault displacement and at short distances (2-10 m) along individual faults. Variations in fault-rock thickness and associated cataclasis have the potential to modify the hydraulic properties of faults and may need to be accounted for in fault-seal analysis.

Keywords: normal faults, cataclasis, silt smear, fault-rock thickness, fault gouge, permeability

Introduction

The grain sizes and permeabilities of fault rocks within siliciclastic sequences are generally lower than sandstones in the adjacent wall rock. The study of these fine-grained fault rocks is typically motivated by a desire to understand better fault evolution (Hull, 1988; van der Zee and Urai, 2005; Childs et al., 2009; Noorsalehi-Garakani et al., 2013), fault-strength properties and the conditions required for slip (e.g., Byerlee, 1978; Morris et al., 1996; Zhang et al., 2009), and how low-permeability fault-rock impacts the movement of fluids in the sub-surface (Knipe, 1992; Antonellini and Aydin, 1994; Yielding et al., 1997; Fisher and Knipe, 2001; Childs et al., 2007). Many studies have demonstrated that fault surfaces displacing siliciclastic sequences can trap migrating hydrocarbons on geological timescales and compartmentalise hydrocarbon reservoirs during production (see Manzocchi et al., 2010). In such cases particular attention has been given to understanding the factors that control the formation of fine-grained fault rocks. Many physical and chemical processes can contribute to the generation of fine-grained fault rock in siliciclastic sequences under brittle failure, with cataclasis and progressive comminution of wall rock during slip and 'smearing' of fine grained wall rocks into the fault zone generally considered to be the most important (Fig. 1).

In the brittle upper crust cataclasis has long been considered critical for the generation of silt- and clay-size particles in fault rock (e.g., Borg et al., 1960; Engelder, 1974; Mandl et al., 1977; Sibson, 1977; Robertson, 1983; Lucas and Moore, 1986; Chester and Logan, 1987; Sammis et al., 1987; Menédez et al., 1996; Gibson, 1998; Cashman and Cashman, 2000; Rawling and Goodwin, 2003; Heilbronner and Keulen, 2006; Keulen et al., 2007; Balsamo and Storti, 2010; Ballas et al., 2012; Exner and Tschegg, 2012; Kristensen et al., 2013; Lommatzsch et al., 2015). At shallow depths (e.g., <5 km) faulting produces breccia, gouge and cataclasites by fracturing, shear and communition of protolith, which may be associated with chemical processes, including grain dissolution and secondary mineralisation (e.g., Knipe, 1993; Fossen et al., 2007). In sedimentary rocks and some unlithified sediments individual grains are broken and disaggregated during fault shearing, which promotes reduction of particle size, increase in particle angularity and collapse of macroscopic pore space (Sammis et al., 1987; Power et al., 1988; An and Sammis, 1994; Cashman and Cashman, 2000; Rawling and Goodwin, 2003; Heilbronner and Keulen, 2006; Fossen et al., 2007; Kaproth et al., 2010; Ballas et al., 2012; Kristensen et al., 2013).

Smearing typically forms where mudstones are sheared into fault zones in a ductile fashion producing a range of smear geometries from classical tapering shear-zone forms to highly irregular thicknesses independent of distance to the source bed (e.g., Bouvier et al., 1989; Lindsay et al., 1993; Lehner and Pilaar, 1997; Childs et al., 2007; Noorsalehi-Garakani et al., 2013; Vrolijk et al., 2016). It is widely accepted that smears can account for dramatic reductions in fault-rock permeability (>4 orders of magnitude) and that fault-seal potential can be calibrated via algorithms proposed to describe the relationships between the thickness and locations of shale smear, the thicknesses of shale source beds and fault displacement (e.g., Bouvier et al., 1989; Lindsay et al., 1993; Knipe, 1997; Lehner and Pilaar, 1997; Fulljames et al., 1997; Yielding et al., 1997, 2010; Manzocchi et al., 1999, 2010; Rivenæs and Dart, 2002; Sperrevik et al., 2002; Bense and Person, 2006; Childs et al., 2007; Jolley et al., 2007; Freeman et al., 2008; Faulkner et al., 2010; Pei et al., 2015; Vrolijk et al., 2016). In contrast, cataclasis of sandstone commonly manifests as deformation bands with relatively modest reduction in permeability (1 to 4 orders of magnitude lower permeability) which is only likely to have a significant impact on permeability when they occur in high densities close to large faults (e.g., Walsh et al., 1998).

Nevertheless, in mixed clastic sequences the porosity and permeability properties of faults with displacements greater than bed thicknesses are likely to be determined by the properties of fault rock generated by both cataclasic and smearing mechanisms. The relative contributions of cataclasis and smear for the generation of fine-grained fault rock is extremely difficult to evaluate. Similarly, how the importance of these processes varies over fault surfaces and with increasing displacement, and to what extent this variability results in changes of fault-rock thickness and hydraulic properties remains unresolved. In this paper we attempt to evaluate the relative contributions of cataclastic and smearing processes to the reduction in grain size in a mixed sequence of siltstones and sandstones.

Grain-size distributions within cataclastic fault rocks and the factors that control them have been extensively studied for granitic rocks and sandstones (e.g., Borg et al., 1960; Engelder, 1974; Robertson, 1983; Chester and Logan, 1987; Sammis et al., 1987; Blenkinsop, 1991; Cashman and Cashman, 2000; Ballas et al., 2012; Exner and Tschegg, 2012; Kristensen et al., 2013; Lommatzsch et al., 2015), although surprisingly few papers explicitly consider the grain-size changes between fault rock and the original source beds in mixed clastic sequences. Heynekamp et al. (1999) compared grain-size distributions for fault rocks and wall rocks associated with growth faults in the Albuquerque Basin, New Mexico, USA, however, in this cases high displacements make it difficult to relate fault rocks directly to their source beds in the wallrock sequence. To overcome this short-coming we study faults where it is possible to directly compare fault rock and the source host rock it was derived from to determine how grain populations in the host rock evolve in response to fault displacement. In the literature the processes that cause the formation of these fine-grained fault rocks have been observed for a range of fault sizes (e.g., Heynekamp et al., 1999; Childs et al., 2007) and are here assumed to be scale independent, making the conclusions of this paper widely applicable.

In this paper we investigate the relative importance of cataclasis and smearing in the production of low-permeability fault-rock along small normal faults with 0.001 to 70 m vertical displacements in weakly lithified Late Miocene turbidites of the Mount

Messenger Formation (MMF) in New Zealand (Fig. 2). These faults from the Taranaki Basin typically comprise a range of structures and rock types including deformation bands, siltstone smear, slip surfaces and fault gouge (Childs et al., 2007; Nicol et al., 2013)(Figs 3-5). Faults have been examined over scale ranges from individual grains (~0.1-350 µm) to the height of the cliffs (~10-20 m) in which they outcrop using analysis of thin sections, SEM images, particle size distribution (PSD) measurements and outcrops of faults mainly in cross section. Inspection of small faults in Taranaki indicates that the main processes that contribute to the generation of fine-grained fault rock are cataclasis of sandstones and smearing of siltstones into the fault (Childs et al., 2007; Nicol et al., 2013). Data presented in this paper provide a basis for assessing the degree to which cataclasis contributes to fault-rock generation, and how comminuted material evolves spatially and temporally. The results complement Childs et al. (2007) who considered the potential impact of silt smears on across-fault sand connectivity and fault-rock permeability from the MMF. These smears are here referred to as silt smears and exhibit geometries typical of shale smears which are widely reported in the literature (e.g., Lindsay et al., 1993; Lehner and Pilaar, 1997; van der Zee and Urai, 2005; Færseth, 2006). Fine grained fault rocks within the MMF can have low permeabilities (e.g., <0.0005 mD; Childs et al., 2007), similar to those for the siltstones and in this respect are equivalent to the shale smears more widely reported in the literature. The MMF in the Taranaki Basin is ideal for this study as it comprises interbedded sandstone and siltstones, the individual lithologies having distinct grain-size distributions that are consistent between beds. This paper supports the view that cataclastic processes make a significant contribution to fault rock generation in mixed clastic sequences and have the potential to influence the hydraulic properties of faults.

Geological setting, data and methods

Fault-rocks and their distribution have been examined for small normal faults (0.001 to 70 m vertical displacement; e.g., Figs 3-5) exposed in coastal cliffs along the eastern margin of the Taranaki Basin, North Island, New Zealand (Fig. 2). These normal faults mainly formed between 2 and 6 Ma due to rifting possibly associated with rollback and/or steepening of the underlying subducting Pacific plate (King and Thrasher, 1992, 1996; Nicol et al., 2005, 2007; Giba et al., 2010, 2013; Seebeck et al., 2014). The exposed faults displace weakly lithified Late Miocene (~7-11.5 Ma) deep-water turbidites of the MMF and are thought to have developed at shallow depths in the crust (<1.5 km) and low confining pressures (e.g., <40 MPa) (King et al. 1993, 2007; Browne et al., 1996, 2005, 2007; King & Thrasher 1996; King and Browne, 2001; Browne and Slatt, 2002). We mainly focus on cross sections of normal faults (N>800 with displacement ≥1 mm) exposed in ~4 km long coastal cliffs ~10-20 m high from Tongaporutu River south (e.g., Fig. 2c). These faults displace a range of lithofacies from thickly bedded (1-5 m) sandstones to interbedded thin (<30 cm) sandstones and siltstones (e.g., King et al., 1993, 2007; Browne et al., 1996, 2005, 2007; Browne and Slatt, 2002)(e.g., Figs 3-5). The source beds for siltstone smear and cataclastic fault rocks (i.e., fault rocks developed by grain comminution) can be identified in many cases making it possible to document changes in the PSD, grain shape and fault-rock structure which arise from varying amounts of displacement and for different types of protolith (i.e. sandstone or siltstone). The present study focuses on sandstone-dominated intervals where thin (<20 cm) siltstone beds typically have average spacings of > 0.5m and sand-on-sand contact across faults is common (Fig.

3). In many cases these sand-on-sand contacts have not been passed by siltstone beds (e.g., PSD samples 3, 5, 7 & 11 in Fig. 3a) and the formation of fault rock can be attributed to processes other than silt smear (e.g., cataclasis).

The importance of cataclasis for fault rock generation and the mechanics of grain destruction are dependent on the texture and composition of the protolith (e.g., Rawling and Goodwin, 2003; Exner and Tschegg, 2012). MMF sandstones comprise silty fine to very fine sands, while the siltstones are primarily sandy silts. Protolith sandstones in the MMF generally have modal grain sizes of ~90-110 µm with ~55-85% sand-, ~15-40% silt- and ≤5% clay-sized particles (Browne and Slatt, 2002; Browne et al., 2005; Fig. 6a). These proportions contrast with those of the siltstone beds which have a grain-size mode of 5-10 µm, ~10-30% sand-, ~65-85% silt- and ≤20% clay-sized particles (Fig. 6b); throughout this paper clay refers to grain size (>2 µm, International Scale) rather than mineralogy. Sandstones and siltstones are mainly very poorly to poorly sorted (sandstones typically have better sorting than siltstones) and comprise sub-rounded to sub-angular grains. Sandstone and siltstone porosities are 30-35% and 20-30%, respectively (Browne et al., 2005). Sandstones primarily comprise ~55-80% lithics (mostly of metamorphic and sedimentary origin; Browne et al., 2005), 20-40% quartz, and 10-30% feldspar (<1% muscovite and biotite). Both the lithics and feldspar sand-sized grains are frequently altered, or partly altered, to phyllosilicates (Childs et al., 2007) which is likely to weaken the grains that, together with the general absence of intergrain cementation and the high porosity, contribute to the low unconfined compressive strengths of the sandstones and siltstones (~3-10 MPa; N. Perrin unpublished data, 2012).

Faults typically comprise zones that accommodate heterogeneous shear strains (Wallace & Morris, 1986; Caine et al., 1996; Childs et al., 1996, 2009; Kim et al., 2004; Wibberley et al., 2008; Faulkner et al., 2010). The highest shear strains are generally focused within or at the margins of fault rock that mainly comprises fault gouge and/or cataclasite. Fault rock in the MMF varies in content and thickness depending on the protolith, fault-zone structure and finite displacement (Childs et al., 2007, 2009; Nicol et al., 2013)(Figs 3-5). Fault rock up to 1 m thick is generally dominated by clay- and silt-sized particles with brecciation and mineralisation rarely observed at outcrop scale. In sandstone-dominated lithologies and for small displacement faults (e.g., <7 m) the majority of fault rock (≥70%) is often contained within thin (typically <10 mm) cataclastic deformation bands, which are typically coloured white to light grey (as opposed to the dark grey of the unweathered sandstone beds)(Fig. 4). Deformation bands generally form anastomosing networks which are widest and contain the greatest number of bands at irregularities (e.g. steps or bends) on faults (Nicol et al., 2013). Fault gouge containing mainly silt- and clay-sized particles is also widely observed. It is either malleable and light grey in colour or forms harder dark grey seams up to 10s of centimetres thick (Figs 4b, 4c & 5). In some cases fine-grained fault rock can be traced to a siltstone source bed, which has been sheared along the fault to produce a silt smear with destruction of the original sedimentary fabric (Fig. 5a & b). Whatever the precise mechanism of fault-rock generation, there is a positive correlation between the thickness of fault rock and displacement (Fig. 7), which in the literature is most often attributed to shearing or attrition of wall rock (Robertson, 1983; Scholz, 1987; Hull, 1988; Power et al., 1988; Sagy et al., 2007), and/or to the amalgamation of shale smears (Bouvier et al., 1989;

Lindsay et al., 1993; Sperrevik et al., 2002; Childs et al., 2007; Vrolijk et al., 2016)(Fig. 1).

The dimensions, evolution and mechanical processes underlying fault-rock formation have been studied here using a combination of techniques including; field mapping, analysis of thin sections (e.g., Fig. 8) and SEM images (e.g., Fig. 9), and particle-size distribution (PSD) measurements (Figs 6, 10, 11 & 12). Field studies include mapping fault-zone geometries and fault-rock thicknesses along individual faults as well as measuring fault-rock and fault-zone thickness for faults with a range of displacements, shear strains and rock types (Figs 3 & 7).

PSD measurements have been widely used in the literature to estimate the contribution of cataclastic processes to the production of fault rock (Engelder, 1974; Sammis et al., 1987; Blenkinsop, 1991; Heynekamp et al., 1999; Balsamo and Storti, 2010; Kristensen et al., 2013; Lommatzsch et al., 2015). In many previous studies however, it was not possible to identify the protolith, and the PSD was not measured for both the source beds and the fault rock. In this paper the PSD of both fault rock and its unfaulted protolith have been measured to determine the extent of cataclasis for 12 faults with displacements between 1.5 mm and 3.3 m (Fig. 11). These direct comparisons between protolith and corresponding fault rock permit the protolith to be inferred from fault rock PSDs for a further 15 faults where displacements are too large (up to 70m) to allow fault rocks to be correlated to their source beds as discussed below (Fig. 12). The PSD dataset comprises a total of 38 unfaulted protolith (20 sandstone and 18 siltstone samples, Fig. 6) and 51 fault rock (28 deformation bands, 15 fault gouge and 8 silt smear, Figs 10-12) samples which were measured using laser-diffraction particle size analysers.

Laser particle size analysers employ the laser diffraction method and for this study generate PSD measurements for grain diameters from 0.063 to 840 µm. Each sample was analysed at least three times with the average presented here (Figs 6, 10, 11 & 12). The sample preparation procedure included gentle sample disaggregation, immersion in 10% H_2O_2 solution and agitation in a heated (~85ºC) ultrasonic water bath for 30 minutes to 1 hour. Increasing the duration of immersion and agitation to time intervals up to 24 hours did not significantly change the PSD for individual samples. Particle diameters for each sample typically range from 0.25 to 350 µm, significantly higher than the lower resolution limit of measurements (0.063 µm). Therefore, the grain-size distributions, which can be highly variable between the faults and their protoliths (Figs 10-12), are unlikely to have been influenced by sample preparation or measurement limitations. The results of the particle-size analysis have been tested by measuring grain sizes from thin section photo micrographs and SEM backscatter images. These photo micrographs and SEM images were acquired for both fault rock (Figs 8 & 9b-c) and undeformed protolith beds (Figs 8 & 9a).

Fault rock in the MMF is primarily generated by cataclasis and silt smear (ductile flow) of sandstone and siltstone protoliths, respectively (Figs 3-5). The contribution of these two processes may vary between faults, between locations on the same fault and through time. How each of these faulting processes modifies the textural and structural fabric of protolith is considered separately in the following two sections, while the temporal and spatial links between these mechanisms are considered in the fault-rock evolution section.

Cataclasites

Cataclasis has been widely observed within fault zones of the MMF (Figs 3-9). Thin sections and SEM images of deformation bands universally demonstrate that particle-sizes are smaller and that there has been macroscopic porosity collapse within fault rock compared to undeformed protolith sandstone (Figs 8 and 9). Each of the three primary grain compositions (quartz, feldspar and lithics) showed grain fragmentation during faulting, although the shear strains at which particle-size decrease occurred varied with composition. Communition of sand-sized particles (mainly ~70-150 µm) is assisted by many of the lithics comprising sub-grains and/or phyllosilicates formed by alteration of feldspars and lithics. Fragmentation was also promoted by some of the quartz, feldspar and lithic grains being fractured prior to measureable shearing (see Fig. 9a unfaulted sandstone). Grains may have fractured prior to the onset of faulting by a number of processes including; (i) sub-resolution (at outcrop scale) wallrock strains (<30 cm from the fault zone) associated with fault initiation and subsequent slip i.e. within the fault process zone, (ii) compaction due to burial by up to 1.5 km of overlying strata and/or, (iii) grain deformation prior to erosion, transport and deposition of Mount Messenger sediments. From the onset of shearing the lithic grains start to disaggregate into their component sub-grains with widespread fracturing at the boundaries between sub-grains. The break up of feldspar grains with abundant phyllosilicate alteration is achieved by transgranular fractures which often utilise cleavage planes and/or zones of phyllosilicate alteration along these planes

(Fig. 8b & c red arrows highlight fractures). Communition of lithic and altered feldspar grains commences at low shear strains (<1) both within the MMF (Dewhurst et al., 2007; this study) and in strata from elsewhere comprising lithic grains (e.g., Exner and Tschegg, 2012). In the present study area lithic and feldspar grains are often broken up or unrecognisable after small displacements of 1-2 mm across thin (< 2 mm) deformation bands and shear strains of <2 across both deformation bands and sheared sandstone beds (e.g., Fig. 9b). Initial disintegration of the weaker grains after millimetres of displacement is associated with pore-space collapse (i.e., a decrease in the size of pores) and an associated reduction of the bulk macroscopic porosity (compare Fig. 9a & b). Quartz and unaltered sand-sized feldspar grains (~70-350 µm) are also fragmented by faulting and, in some cases, appear to become more rounded with increasing shear strain (Fig. 8b & d, white arrows highlight rounded grains). Grain fragmentation may be assisted by pre-shear fractures, while rounding could arise from particle flaking or spalling associated with intergrain collisions during shear events (Hooke and Iverson, 1995; Rawling and Goodwin, 2003). After shear strains of about 1-2 these stronger grains are generally enclosed in a clay-silt matrix produced by destruction of the weaker grains (e.g., Fig. 9b & c), which may partly buffer the remaining sand-sized particles from collision. Despite this buffering, grain-size reduction of sand-sized particles continues with increasing shear strains and displacement (compare Fig. 9b & c).

PSD measurements for fault rock demonstrate decreases in particle size compared to known (Fig. 10 and 11) and inferred sandstone protoliths (Fig.12a). In all cases where the PSD of a sandstone protolith is known, the particle-size reduction due to shear is achieved by an increase in the component of silt- (2-63 µm) and clay-sized (<2 µm, International scale) particles at the expense of the sand fraction (>63 µm)(Figs 10, 11a-h & 12a). This particle-size reduction is not accompanied by a change in the limits of the faulted particle-size population. Instead, adjustments in the PSDs are mainly characterised by a decrease in the dominance of the 90-110 µm mode in the parent sandstone and a comparable increase in the prominence of a silt mode at ~5-10 µm. In some deformation bands these changes produce bimodal grain size populations with sand and silt modes (Fig. 11e-h). The magnitude of change in the PSD varies between samples from cases where departure of the fault-rock PSD from the sandstone grain-size population is minor (e.g., Fig. 11a-c) to samples where the grain sizes approach those of the siltstone beds (e.g., Fig. 11g-h). These variations could be attributed to a number of factors including, variations in the proportion of sand-sized particles and weak grains in the protolith, increases in shear strain (see Fault-rock evolution section), and perhaps also to sampling artefacts. Greater proportions of sand-sized grains are likely to increase the number of contact points between these grains and the number of weaker grains available for breakup into their sub-grains, both of which promote cataclasis. Thin section and SEM observations support the notion that for some deformation bands particle size decreases with increasing displacement (see Figs 8 & 9). This conclusion is not consistent with Fig. 11a-h which show PSD data for a range of fault displacements and suggest that the negative relationship between particle size and displacement is not universal. The discrepancy between micro observations (SEM images and thin sections) and some PSD measurements could be influenced by variations in the degree of shear localisation within individual samples/faults and/or by sample contamination by grains from unsheared sandstone between deformation bands that are not visible in hand specimen.

PSD data support the suggestion that some fault gouges which, in hand specimen do not appear to contain deformation bands and are superficially similar in colour and texture to siltstone beds, may also have formed by cataclasis of sandstone protoliths. For the fault gouges in Fig. 12a (black lines) the protolith is unknown but it may be possible to infer the protolith from the PSDs which, in each case, comprise a sand-sized mode of 90-110 µm and a significant proportion of silt (~45-65%). The high proportion of sand-sized particles in these fault rocks is inconsistent with them being largely or entirely derived from shear or injection of siltstone beds into the fault zones (unless significant sand-silt mixing occurs for which there is little direct evidence). The PSDs in Fig. 12a are comparable to the average PSD for deformation bands (thick grey line Fig. 12a), and we propose that these gouges may have primarily developed due to cataclasis induced by distributed shear of sandstone beds within fault zones. Within these high strain zones internal structure in the form of, for example deformation bands, is not visible but the earlier existence of deformations bands in these zones of distributed grain communition cannot be ruled out. As is the case for deformation bands, distributed shearing of sandstone initially results in the fracturing and destruction of the weaker lithic and altered feldspar grains followed by breakup of quartz and unaltered feldspar. The shear strains required to produce particle-size reduction by distributed shear may be similar to that of deformation bands. Because zones of fault gouge may be orders of magnitude wider than individual deformation bands the total displacement required to produce a comparable grain-size reduction may be orders of magnitude larger.

The observed changes in PSD between protolith and sheared sandstones are consistent with cataclasis seen in SEM and thin section (Figs 8 & 9) and with the literature (e.g., Aydin, 1978; Antonellini and Aydin, 1994; Rawling and Goodwin, 2003; Fossen et al., 2007; Kristensen et al., 2013), in suggesting that cataclasis is an important component of the faulting process in sandstones. Cataclasis generally produces PSDs that are intermediate between those of the sandstone protolith and siltstone beds (e.g., Figs 10, 11a-h & 12a). In rare cases the PSD of fault rock derived from sandstone may approach that of siltstones (Figs 11g & h, 12a), and in such instances the origin of the fault rock can only be determined if the source of protolith material is unambiguous (refer to Silt Smear section for further discussion). The similarity of PSDs for siltstone beds and fault rock with modes at 5-10 µm and ranges of ~0.1-350 µm (Figs 10 & 11) indicate that factors common to both rock types (i.e. fault rock and siltstone) may control their PSDs. It is also possible that for faults the stability of the lower bounds of the PSDs ~0.1 µm records a grinding limit of fault rock derived from the MMF, as has been proposed by An and Sammis (1994) for a 1 µm minimum particle size in fault rock from California (see also Keulen et al., 2007). However, the grinding-limit hypothesis does not explain why siltstone and fault rock PSDs should have comparable lower limits. An alternative explanation is that both fault rock and siltstone are derived from the breakdown of sandstone grains of similar composition and with comparable populations of defects (e.g., sub-grain boundaries, fractures, cleavages and zones of alteration). For such a hypothesis the lower limit of particle size is partly controlled by the density of defects and the size of sub-grains within the parent sand grains.

Silt Smear

Smear of fine-grained beds reflects ductile deformation (at outcrop scale) of silt- and clay-rich beds and may be achieved by intergranular sliding and/or micro-faulting without significant cataclasis (Knipe, 1993; Lindsay et al., 1993; Yielding et al., 1997; van der Zee and Urai, 2005; Egholm et al., 2008; Noorsalehi-Garakani et al., 2013; Pei et al., 2015; Vrolijk et al., 2016). Smear of siltstone beds is common in the MMF where it is often dark grey and similar in colour to unweathered siltstone source beds (e.g., Figs 3b, 4b, 5a & b; see also Figs 3c, 4b and 7 in Childs et al., 2007). Amalgamated silt smears from multiple source beds and individual silt smears produced by a single bed are both observed or inferred from fault outcrops of MMF. We mainly focus on individual silt smears that can be unambiguously correlated with a source bed and use the results of PSD analysis to draw inferences about the origin of fault gouge where the source beds are unknown.

Globally previous studies have shown that shale smears can be thicker closer to the source bed, increase in thickness with source-bed thickness and decrease in thickness with rising total displacement (Lindsay et al., 1993; Færseth, 2006). Within the MMF the thickness and dip-parallel continuity of silt smears is highly variable (Fig.3b, 4b & 5a). These thickness variations are often controlled by the locations and numbers of slip surfaces which displace the silt smear (e.g., Childs et al., 2007)(Fig. 5b inset). In Fig. 10, for example, siltstone bed A is smeared across the entire thickness of the fault zone (an interpretation confirmed by comparison of PSDs for samples 2, 3, 5 & 13, see Fig. 10), with variations in smear thickness from ~3 to 30 mm that occur primarily across slip surfaces and are not correlated with distance from the source bed outside of the fault zone. The role of minor internal faults in the shear of siltstone beds across fault zones is observed in thin sections and in outcrop. In Fig. 5b (inset), for example, the geometry of a siltstone smear is influenced by small-scale-faulting. Where these small scale faults are not readily seen at outcrop scale they produce an apparently ductile smear but it is possible that they are associated with minor cataclasis.

The PSD of siltstone source beds and associated silt smears indicate that significant grain-size reduction and cataclasis does not occur within silt smears in the MMF. Comparison of the grain sizes for silt smears and their undeformed protolith beds in the MMF suggests that, where the source beds and smears can be unambiguously correlated, the two populations are similar (e.g., compare samples 2, 3, 5 & 13 in Fig. 10; see also Fig. 11i-l). For each of the faults presented in Fig. 11i-l a small (<~5%) increase in the volume of very fine silt to clay (e.g., <4 µm) may accompany silt smear. These minor grain-size reductions could reflect cataclastic processes associated with the formation of micro-faults best observed in thin sections. In addition some samples show a slight increase in the proportion of sand-sized grains (Fig. 11j) and in such cases it is possible that silt smear was accompanied by minor mixing with adjacent sandstone beds. The lack of significant grain size reduction by fragmentation is consistent with the notion that on the grain scale, silt smear is mainly accommodated by intergranular sliding facilitated by the high proportion (70%) of clay- and silt-sized fractions. The high proportion of the silt- and clay-sizes also reduces the probability of larger silt- and sand-sized grains of quartz and feldspar colliding during shear events decreasing the likelihood of particle size reduction arising from these impacts (e.g., Sammis et al., 1987).

PSD data also indicate that some fault gouges derived from an undetermined protolith may have formed by silt smearing. Figure 12b shows the PSD for 6 fault gouges (thin black lines) together with the average PSD for sandstone and siltstone beds (thick red lines) and the average PSD for silt smears where the source bed is known (thick grey line). Unlike the grain sizes for fault rock in Fig. 12a the gouges in Fig. 12b do not contain the ~100 µm mode apparent in the sandstones and deformation bands and the fault gouge is inferred not to be derived from sandstone protolith. Instead, while there is some variability in PSD between different fault gouges, they generally match the average particle sizes of siltstone beds and silt smears sourced from siltstone protoliths. While it is possible that these fault gouges reflect extreme cataclasis, analysis of cataclastic fault rock suggests that such extremes are rarely achieved (Figs 10-12a). Therefore, we suggest that the fault gouges in Fig. 12b could have formed mainly by smear and drag of siltstone beds into fault zones with little change in the PSD.

Discussion

Fault-Rock Evolution and Variability

In the brittle crust fault zones are typically inferred to form as part of a strain weakening and slip localisation process (Sibson, 1977; Sagy et al., 2007; Childs et al., 2009; Rotevatn and Fossen, 2012; Nicol et al., 2013) and, as a consequence, the PSD, architecture and thickness of fault rock evolves with increasing cumulative displacement. These changes primarily reflect increased shear strains that result in the progressive destruction of irregularities on fault surfaces, the incorporation of wall rock into fault zones and, for siliciclastic sequences, the comminution of individual grains and smear of shale beds along faults (e.g., Power et al., 1988; Scholz, 1987; Childs et al., 1996; 2009; Sagy et al., 2007; Nicol et al., 2013). In weakly lithified strata of the MMF both cataclasis and silt smear are common (e.g., Figs 3, 4, 5, 10, 11 & 12). Based on the data collected, fault-rock evolution in the MMF is interpreted to be mainly dependent on three key factors; (i) the initial geometry of the fault surface which strongly controls fault-zone thickness and complexity, (ii) fault displacement and the associated shear strains imposed on the protolith and, (iii) the particle size of faulted protolith which influences the relative contributions of cataclasis and intergranular sliding in fault-rock production.

Global data suggest that fault-rock thickness and fault-zone complexity are strongly controlled by the locations of irregularities on a fault surface. From the onset of slip, strains are more distributed at irregularities than on the intervening relatively straight segments and, as a result, fault rock development (i.e. thickness and PSD) is likely to vary over an individual fault surface (Childs et al., 2009; Nicol et al., 2013). Intervening segments for small faults, including those that displace the MMF, are characterised by a relatively narrow fault-rock thickness (<10 mm) within which slip localises rapidly. At fault irregularities the increase in fault-rock thickness with rising displacement reflects their progressive destruction associated with rising shear strains and migration of incremental shear towards an optimal, energetically-efficient planar geometry, where slip is focused into a primary through-going zone of fault rock or onto a surface. The cumulative displacement at which an irregularity is bypassed depends on the dimensions of the irregularity and the size of the fault; as the ratio between irregularity width and size of the average incremental displacement decreases so too does the longevity of the irregularity (e.g., Power et al., 1988; Childs et al., 1996, 2009; Sagy et al., 2007; Nicol et al., 2013). For example, an individual small fault with a cumulative displacement of 0.5 m and slip increments of millimetres will breach millimeter-scale irregularities more rapidly than metre-scale structures. The asperity removal process creates fault-bound lenses (e.g., Childs et al., 1996; van der Zee and Urai, 2005; Awdal et al., 2014) which, for the faults studied here range in thickness from millimeters to meters. These lenses form part of fault zones and may be bypassed by subsequent faulting or sheared along the fault contributing to the generation of fine-grained fault rock (e.g., Childs et al., 1996, 2009; Watterson et al., 1998; Bonson et al., 2007).

Shearing and breakup of irregularities may in part account for the thickening of fault rock with increasing displacement which can be observed in displacement-fault rock thickness plots (Robertson, 1983; Scholz, 1987; Hull, 1988; Blenkinsop, 1989; Marrett and Allmendinger, 1990; Knott, 1994; Little, 1995; Childs et al., 2007, 2009). A similar weakly positive relationship between fault-rock thickness and displacement was observed for the faults in this study where the ratio of these values ranges from 1 to 1000 (Fig. 7). At a given displacement cataclastic and silt-smear processes are capable of producing fault-rock thicknesses that span much of the range of values for all faults observed in the MMF (Fig. 7b). Similarly, the range of fault-rock thickness for an individual fault, sampled on a 2-10 m long profile, can account for a significant proportion (e.g., >20%) of the range in fault-rock thickness for all faults within the MMF for a given displacement (bars in Fig. 7a represent the range of observations for each fault profile). In Figure 13, for example, fault-rock thickness varies from 2-17 mm, which is about one third of the ~0.5-50 mm thickness range for faults with ~7.5 cm displacement in Fig. 7a. The range of fault-rock thicknesses for individual faults were typically recorded over dip lengths of 2-10 m which, based on the displacement-length relationships of faults (e.g., Walsh and Watterson, 1988; Schlishe et al., 1996), may constitute <5% of the total dip dimension of the fault surfaces. Therefore, the variations of fault-rock thickness for individual faults in Fig. 7a are a minimum for the range over the entire fault surface with the total spread of data in Fig. 7a being a possible maximum for individual faults. These variations in fault-rock thickness may have implications for fault porosity and permeability properties and are discussed further in the next section.

The mechanism by which protolith material is converted to fault rock in the MMF is strongly dependent on its original grain size. Sandstones initially deform mainly by cataclasis with intergranular sliding inferred to become increasingly important as the clay- and silt-sized fraction rises, while siltstones mainly accommodate shear by intergranular sliding from the onset of faulting (Figs 9 & 11). The communition of sand-sized particles is interpreted to occur both in response to localised shear within deformation bands and to distributed shear across lenses of sandstone. The PSD for deformation bands and distributed sandstone shear are comparable (i.e. with a sand-sized mode and a significant proportion of silt)(Figs 11a-h & 12a). Deformation bands display intense communition of grains at relatively low shear strains (e.g. 1.4 in Fig. 9b) and less marked grain size reduction at higher finite values (e.g. a shear strain of 70 in Fig. 9c). Rapid initial comminution reflects the presence of weak lithic and altered feldspar grains which constitute up to ~70% of the protolith sandstone grains and experience significant disaggregation at low shear strains <2. Differences in the PSD of fault rock at 1.5 mm and 65 mm displacement suggest that even for deformation bands cataclasis can continue after this initial stage of shear (compare

Fig. 9b & c). In addition, the migration of the locus of deformation within fault irregularities (Nicol et al., 2013), shear of sandstone lenses along fault surfaces and the progressive incorporation of sandstone wallrock into fault zones will mean that cataclasis continues to contribute to fault-rock formation. With increasing displacements the quartz and unaltered feldspar grains are comminuted more slowly, partly because they are stronger (than the lithic and altered feldspar grains), but also because the clay-silt matrix derived from destruction of the weaker grains accommodates distributed shear and buffers the collision of stronger sand-sized grains. Overcoming the buffering effect of the matrix could be facilitated by high shear-strain rates during discrete slip events of coseismic origin. Cataclasis in response to earthquake slip is consistent with the occurrence of deformation bands within unconsolidated sands in active fault zones close to the San Andreas Fault in California (Cashman and Cashman, 2000; Cashman et al., 2007).

A transition from cataclasis to intergranular sliding is indicated by the stability of PSDs for finer grain size fault rocks produced by silt smear. As cataclasis is in large part achieved by fragmentation of sand-sized particles, the transition can be related to the proportion of sand-sized particles in the fault rock. Sheared siltstone beds that are inferred to have primarily deformed by intergranular sliding contain ~10-30% sand-sized particles (average ~15%), which is similar to undeformed siltstones (Figs 6, 10-12). Sandstone protoliths typically contain ~50-85% sand-sized particles which in most cases decreases to ~35-50% following cataclasis. Therefore, the available particle-size data can be interpreted to suggest that intergranular sliding and cataclasis dominate in fault rock with ≤30% and ≥50% sand-sized particles, respectively.

Implications for Fluid Flow

Techniques for estimating fault-seal potential, including juxtaposition analysis (Allan, 1989; Knipe, 1997) and shale-smear algorithms (Bouvier et al., 1989; Lindsay et al., 1993; Yielding et al., 1997, 2010; Manzocchi et al., 1999, 2010; Sperrevik et al., 2002; Yielding, 2002; Childs et al., 2007), do not specifically account for grain-size reduction during cataclasic processes. However, in some circumstances cataclasis may have a significant impact on fault hydraulic properties (e.g., fault-rock thickness and permeability) and our ability to successfully predict fluid-flow across and along faults. In the MMF cataclasic processes account for a significant component of the total fault-rock thickness and its variability over fault surfaces. While the impact of cataclasis on faults with displacements less than the bed thickness is clear, evaluating its importance for larger faults is more difficult. Of the faults studied in the MMF with displacements sufficiently large that the fault-rock source material is unknown (displacements of ~ 1 to 70 m), ~60% of the fault gouge samples analysed using PSD (i.e. 9 and 6 faults in Fig. 12a and b, respectively), were indistinguishable from fault rock formed by cataclasis of sheared sandstone. The proportion of sampled fault gouge potentially produced by cataclasic processes is comparable to and, may be a function of, the proportion of sandstone beds in the faulted sequence, which for the MMF is about 60% (Browne et al., 2007). Therefore, cataclastic fault rock could exert a significant control on the porosity and permeability properties of the faults in the MMF, and the role of cataclasites on the fluid-flow properties of faults warrant further investigation.

Existing permeability data for cataclastic fault rocks and sandstones in the MMF are consistent with the view that faulting of sandstones can produce permeability reductions of at least 4 orders of magnitude (e.g., cataclastic fault rocks ≤0.03 mD versus mainly ≥30 mD for sandstones: Browne and Slatt, 2002; Childs et al., 2007; Higgs et al., 2012), that are sufficiently large to retard across-fault flow within sandstone beds.

Conclusions

Cataclasis and silt smear are both observed on small normal faults along the eastern margin of the Taranaki Basin. Cataclasis primarily occurs in sandstone protoliths resulting in disaggregation of sand-sized grains (mode ~90-115 µm) and production of silt (mode ~5-25 µm) without changes in the total spread of the grain size population. Intense cataclasis starts at very low shear strains of <2 (fault displacements ~1.5 mm) and is facilitated by the presence of weak lithics and altered feldspar grains which break up easily. By contrast, the presence of clay and silt-sized particles inhibits fragmentation. Therefore, smear of siltstone beds does not produce significant grain-size reduction and is primarily achieved by intergrain slip and micro-faulting. Despite the occurrence of silt smear, cataclasis can account for >50% of the total fault-rock thickness in sand-silt multilayers. Cataclasis, which is often not explicitly accounted for in fault-seal analysis, has the potential to modify fluid flow near and across faults and may need to be accounted for in fault seal analysis.

Acknowledgements

This research was funded by the GNS Science New Zealand Petroleum Basin Resources programme (A.Nicol), the ITF FIFT programme (A.Nicol, C.Childs) and Tullow Oil plc (C.Childs). Thank you to Geoffrey Rawling and an anonymous reviewer for their constructive comments, which resulted in substantial improvements to the manuscript.

References

Allan, U.S., 1989. Model for Hydrocarbon Migration and Entrapment within Faulted Structures. American Association of Petroleum Geologists Bulletin 73(7), 803–811.

An, L.-j, Sammis, C., 1994. Particle size distribution of cataclastic fault materials from southern California: a 3-d study. Pure and Applied Geophysics 143, 203-227.

Antonellini, M., Aydin, A., 1994. Effect of faulting on fluid flow in porous sandstones: geometry and spatial distribution. American Association of Petroleum Geologists Bulletin 79, 642–671.

Awdal, A., Healy, D., Alsop, G.I., 2014. Geometrical analysis of deformation band lozenges and their scaling relationships to fault lenses. Journal of Structural Geology 66, 11-23.

Aydin, A., 1978. Small faults formed as deformation bands in sandstone. Pure and Applied Geophysics 116, 913–930.

Ballas, G., Soliva, R., Sizun, J.-P., Benedicto, A., Cavailhes, T., Raynaud, S., 2012. The importance of the degree of cataclasis in shear bands for fluid flow in porous sandstone (Provence, France). American Association of Petroleum Geologists Bulletin 96, 2167-2186.

Balsamo, F., Storti, F., 2010. Grain size and permeability evolution of soft-sediment extensional sub-seismic and seismic fault zones in high-porosity sediments from the Crotone Basin, southern Apennines, Italy. Marine and Petroleum Geology 27, 822-837.

Bense, V.F., Person, M., 2006. Faults as conduit-barrier systems to fluid flow in siliciclastic sedimentary aquifers: Water Resources Research 42, W05421, doi:10.1029/2005WR004480.

Blenkinsop, T.G., 1989. Thickness-displacement relationships for deformation zones: Discussion. Journal of Structural Geology 11, 1051-1054.

Blenkinsop, T.G., 1991. Cataclasis and processes of particle size reduction. Pure and Applied Geophysics 136, 59-86.

Bonson, C.G., Childs, C., Walsh, J.J., Schöpfer, M.P.J., Carboni, V., 2007. Geometric and kinematic controls on the internal structure of a large normal fault in massive limestones: the Maghlaq Fault, Malta. Journal of Structural Geology 29, 336-354.

Borg, I., Friedman, M., Handing, J., Higgs, D.V., 1960. Experimental deformation of St. Peter sand: a study of cataclastic flow. In: Griggs, D., Handing, J. (Eds.), Rock Deformation. Geological Society of America Memoirs 79, 133–191.

Bouvier, J.D., Kaarssijpesteijn, C.H., Kluesner, D.F., Onyejekwe, C.C., van der Paul, R.C., 1989. Three-dimensional seismic interpretation and fault sealing investigations, Nun River Field, Nigeria. American Association of Petroleum Geologists Bulletin 73 (11), 1397-1414.

Browne, G.H., Slatt, R.M., 2002. Outcrop and behind-outcrop characterization of a late Miocene slope fan system, Mt. Messenger Formation, New Zealand. American Association of Petroleum Geologists Bulletin 86, 841–862.

Browne, G.H., McAlpine, A., King, P.R., 1996. An outcrop study of bed thickness, continuity and permeability in reservoir facies of the Mt. Messenger Formation, North Taranaki. New Zealand Petroleum Conference Proceedings, 10-13 March 1996, Volume 1. Ministry of Economic Development, Wellington, 154–163.

Browne, G.H., King, P.R., Higgs, K.E., Slatt, R.M., 2005. Grain size characteristics for distinguishing basin floor fan and slope fan depositional settings: outcrop and subsurface examples from the late Miocene Mount Messenger Formation, New Zealand. New Zealand Journal of Geology & Geophysics 48, 213-227.

Browne, G.H., King, P.R., Arnot, M.J., Helle, K., 2007. A complete middle-to-inner basin-floor-fan cycle, Mount Messenger Formation, Tongaporutu, New Zealand. In: Atlas of deep-water outcrops, eds Nilsen, T.H., Shew, R.D., Steffens, G.S., Studlick, J.R.J. American Association of Petroleum Geologists Studies in Geology 56, 245-248, DOI:10.1306/1240947st563302.

Byerlee, J., 1978. Friction of rocks. Pure & Applied Geophysics. 116, 615–626. doi:10.1007/ BF00876528.

Caine, J.S., Evans, J.P., Forster, C.B., 1996. Fault zone architecture and permeability structure. Geology 24(11), 1025-28.

Cashman, S., Cashman, K., 2000. Cataclasis and deformation-band formation in unconsolidated marine terrace sand, Humboldt County, California. Geology 28, 111–114.

Cashman, S.M., Baldwin, J.N., Cashman, K.V., Swanson, K., Crawford, R., 2007. Microstructures developed by coseismic and aseismic faulting in near-surface sediments, San Andreas fault, California. Geology 35, 611–614.

Chester, F.M., Logan, J.M., 1987. Composite planar fabric gouge from the Punchbowl Fault, California. Journal of Structural Geology 9, 621–634.

Childs, C., Nicol, A., Walsh, J.J., Watterson, J., 1996. Growth of vertically segmented normal faults. Journal of Structural Geology 18, 1389–1397.

Childs, C., Walsh, J.J., Manzocchi, T., Strand, J., Nicol, A., Tomasso, M., Schöpfer, M., Aplin, A., 2007. Definition of a fault permeability predictor from outcrop studies of a faulted turbidite sequence, Taranaki, New Zealand. In: Structurally Complex Reservoirs. Geological Society of London, Special Publication 292, 235-258.

Childs, C., Walsh, J.J., Manzocchi, T., Bonson, C., Nicol A., Schöpfer, M.P.J., 2009. A geometric model of fault zone and fault rock thickness variations. Journal of Structural Geology 31, 117-127.

Dewhurst, D., Clennell, B., Strand, J., Underschultz, J., Gartrell, A., Bailey, W., 2007. Clay Rich Fault Gouge in Low Clay Content Reservoirs: Implications for Predictive

Fault Seal Evaluation. AAPG Search and Discover Article #90066©2007. American Association of Petroleum Geologists Hedberg Conference, The Hague, The Netherlands.

Egholm, D.L., Clausen, O.R., Sandiford, M., Kristensen, M.B., Korstgård, J.A., 2008. The mechanics of clay smearing along faults. Geology 36(10), 787-790.

Engelder, J.T., 1974. Cataclasis and the generation of fault gouge. Geological Society of America Bulletin 85, 1515-1522.

Exner, U., Tschegg, C., 2012. Preferential cataclastic grain size reduction of feldspar in deformation bands in poorly consolidated arkosic sands. Journal of Structural Geology 43, 63-72.

Færseth, R.B., 2006. Shale along large faults: continuity of smear and the fault seal capacity. Journal of the Geological Society 163, 741-751.

Faulkner, D. R., Jackson, C.A.L., Lunn, R.J., Schlische, R.W., Shipton, Z.K., Wibberley, C.A.J., Withjack, M.O., 2010. A review of recent developments concerning the structure, mechanics and fluid flow properties of fault zones. Journal of Structural Geology 32, 1557-1575.

Fisher, Q.J., Knipe, R.J., 2001. The permeability of faults within siliciclastic petroleum reservoirs of the North Sea and Norwegian Continental Shelf. Marine and Petroleum Geology 18, 1063-1081.

Fossen, H., Schultz, R., Shipton, Z., Mair, K., 2007. Deformation bands in sandstone - a review. Journal of the Geological Society of London 164, 755–769.

Freeman, S.R., Harris, S.D., Knipe, R.J., 2008, Fault seal mapping; incorporating geometric and property uncertainty. Geological Society Special Publications 309, 5-38.

Fulljames, J.R., Zijerveld, L.J.J., Franssen, R.C.M.W., 1997. Fault seal processes: systematic analysis of fault seals over geological and production time scales. In: Møller-Pedersen, P. & Koestler, A. G. (eds) Hydrocarbon Seals, Importance for

Exploration and Production. Norwegian Petroleum Society, Special Publication, 7, 51–59.

Giba, M., Nicol, A., Walsh, J.J., 2010. Evolution of faulting and volcanism in a backarc basin and its implications for subduction processes. Tectonics 29, TC4020, doi:10.1029/2009TC002634, 2010.

Giba, M., Walsh, J.J., Nicol, A., Mouslopoulou, V., Seebeck, H., 2013. Investigation of the spatio-temporal relationship between normal faulting and arc volcanism on million-year timescales. Journal of the Geological Society of London 170 (6), 951-962. http://dx.doi.org/10.1144/jgs2012-121.

Gibson, R.G., 1994. Fault-zone seals in siliciclastic strata of the Columbus Basin, offshore Trinidad. Association of Petroleum Geologists Bulletin 78, 1372-85.

Gibson, R.G., 1998. Physical character and fluid-flow properties of sandstone-derived fault zones. In: Coward, M. P., Daltaban, T. S. & Johnson, H. (eds) Structural Geology Characterisation. Geological Society London Special Publication 127, 83–97.

Heilbronner, R., Keulen, N., 2006. Grain size and shape analysis of fault rocks. Tectonophysics 427, 199-216.

Heynekamp, M.R., Goodwin, L.B., Mozley, P.S., Haneberg, W.C., 1999. Controls on fault-zone architecture in poorly lithified sediments, Rio Grande Rift, New Mexico: implications for fault-zone permeability and fluid flow. In: Haneberg, W.C., Mozley, P.S., Moore, K.C., Goodwin, L.B., (Eds), Faults and Subsurface Fluid Flow in the Shallow Crust. American Geophyscial Union Geophysical Monograph 113, 27-50.

Higgs, K.E., Strogen, D., Griffin, A., Ilg, B., Arnot, M., 2012. Reservoirs of the Taranaki Basin, New Zealand. Data series No. 2012/13a. Lower Hutt: GNS Science.

Hooke, R.L. Iverson, N.R., 1995. Grain-size distribution in deforming sub-glacial tills: role of grain fracture. Geology 23, 57-60.

Hull, J., 1988. Thickness–displacement relationships for deformation zones. Journal of Structural Geology 10, 431–435.

Jolley, S.J., Barr, D., Walsh, J.J., Knipe, R.J., 2007. Structurally complex reservoirs: an introduction. In: Structurally Complex Reservoirs. (Edited by Jolley, S.J., Barr, D., Walsh, J.J. & Knipe, R.J.). Geological Society of London, Special Publication 292, 1-24.

Kaproth, B.M., Cashman, S.M., Marone, C., 2010. Deformation band formation and strength evolution in unlithified sand: The role of grain breakage. Journal of Geophysical Research 115, B12103, doi:10.1029/2010JB007406, 2010.

Keulen, N., Heilbronner, R., Stünitz, H., Boullier A-M., Ito, H., 2007. Grain size distributions of fault rocks: A comparison between experimentally and naturally deformed granitoids. Journal of Structural Geology 29, 1282-1300.

Kim, Y.-S., Peacock, D.C.P., Sanderson, D.J., 2004. Fault damage zones. Journal of Structural Geology 26, 503-17. doi: 10.1016/j.jsg.2003.08.002.

King, P.R., Thrasher, G.P., 1992. Post-Eocene development of the Taranaki Basin, New Zealand; convergent overprint of a passive margin. In: Watkins, J. S., Zhiqiang, F. & Mcmillen, K. J. (eds) Geology and Geophysics of Continental Margins. American Association of Petroleum Geologists Memoir, 53, 93–118.

King, P.R., Thrasher, G.P., 1996. Cretaceous– Cenozoic geology and petroleum systems of the Taranaki Basin, New Zealand. Institute of Geological and Nuclear Sciences Monograph, Wellington, 13.

King, P.R. Browne, G.H., 2001. Miocene turbidite reservoir systems in Taranaki Basin, New Zealand: established plays and analogues for deep-water exploration: East Australian Basins Symposium, Eds. K.C. Hill & T. Bernecker, 129-139.

King, P.R., Scott, G.H., Robinson, P.H., 1993. Description, correlation and depositional history of Miocene sediments outcropping along the north Taranaki coast. Institute of Geological and Nuclear Sciences Monograph, Wellington, 5.

King, P.R., Browne, G.H., Arnot, M.J., Slatt, R.M., Helle, K., Stromsoyen, I., 2007. An overview of the Mount Messenger-Urenui Formations, New Zealand: 2-D oblique-dip outcrop transect through an entire third-order, progradational, deep-water clastic succession. In: Atlas of deep-water outcrops, eds Nilsen, T.H., Shew, R.D., Steffens, G.S., Studlick, J.R.J. American Association of Petroleum Geologists Studies in Geology 56, 238-240, DOI:10.1306/1240947st563302

Knipe, R.J., 1992. Faulting processes and fault seal. In: Structural and tectonic modelling and its application to petroleum geology, eds Larsen, R.M., Brekke, H., Larsen, B.T., Talleras, E., Amsterdam, Elsevier, 325-342.

Knipe, R.J., 1993. The influence of fault zone processes and diagenesis on fluid flow. In: Diagenesis and basin development, eds Horbury, A.D., Robinson, A.D., American Association of Petroleum Geologists Studies in Geology 56, 135-151.

Knipe, R.J., 1997. Juxtaposition and seal diagrams to help analyze fault seals in hydrocarbon reservoirs. American Association of Petroleum Geologists Bulletin 81(2), 187-195.

Knott, S.D., 1994. Fault zone thickness versus displacement in the Permo-Triassic sandstones of NW England. Journal of the Geological Society 151, 17–25.

Kirstensen, M.B., Childs, C., Olesen, N.Ø., Korstgård, J.A., 2013. The microstructure and internal architecture of shear bands in sand-clay sequences. Journal of Structural Geology 46, 129-141.

Lehner, F.K., Pilaar, W.F. 1997. On a mechanism of clay smear emplacement in synsedimentary normal faults. In: Møller-Pedersen, P. & Koestler, A. G. (eds) Hydrocarbon Seals, Importance for Exploration and Production. Norwegian Petroleum Society, Special Publication 7, 39–50.

Lindsay, N.G., Murphy, F.C., Walsh, J.J., Watterson, J., 1993. Outcrop studies of shale smears on fault surfaces. In: Flint, S. & Bryant, A. D. (eds) The Geological Modelling of Hydrocarbon Reservoirs and Outcrop Analogues. International Association of Sedimentology 15, 113–123.

Little, T.A., 1995. Brittle deformation adjacent to the Awatere strike-slip fault in New Zealand: faulting patterns, scaling relationships, and displacement partitioning. Bulletin of the Geological Society of America 107, 1255–1271.

Lommatzsch, M., Exner, U., Gier, S., Grasemann, B., 2015. Dilatant shear band formation and diagenesis in calcareous, arkosic sandstones, Vienna Basin (Austria). Marine and Petroleum Geology 62, 144-160.

Lucas, S.E., Moore, J.C., 1986. Cataclastic deformation in accretionary wedges: Deep Sea Drilling Project Leg 166, southern Mexico, and on land examples from Barbados and Kodiak Islands. In: Moore, J.C. (Ed.), Structural Fabrics in Deep Sea Drilling Project Cores from Forearcs, Geological Society of America Memoirs 166, 89–104.

Mandl, G., de Jong, N.J., Maltha, A., 1977. Shear zones in granular material. Rock Mechanics 9, 95-144.

Manzocchi, T., Walsh, J.J., Nell, P., Yielding, G., 1999. Fault transmissibility multipliers for flow simulation models. Petroleum Geoscience 5(1), 53-63.

Manzocchi, T., Childs, C., Walsh, J.J., 2010. Faults and fault properties in hydrocarbon flow models. Geofluids 10(1-2), 94-113.

Marrett, R., Allmendinger, R.W., 1990. Kinematic analysis of fault-slip data. Journal of Structural Geology 12, 973–986.

Menéndez, B., Zhu, W., Wong, T-f., 1996. Micromechanics of brittle faulting and cataclastic flow in Berea sandstone. Journal of Structural Geology 18, 1-16.

Morris, A., Ferrill, D.A., Henderson, D.B., 1996. Slip-tendency analysis and fault reactivation. Geology 24(3), 275-278.

Nicol, A., Walsh, J., Berryman, K., Nodder, S., 2005. Growth of a normal fault by the accumulation of slip over millions of years. Journal of Structural Geology 27, 327–342.

Nicol, A., Mazengarb, C., Chanier, F., Rait, G., Uruski, C., Wallace, L., 2007. Tectonic evolution of the active Hikurangi subduction margin, New Zealand, since the Oligocene. Tectonics 26, TC4002, doi:10.1029/2006TC002090.

Nicol, A, Childs, C, Walsh, J.J., Schafer, K., 2013. A geometric model for the formation of deformation bands. Journal of Structural Geology 55, 21-33.

Noorsalehi-Garakani, S., Kleine Vennekate, G.J., Vrolijk, P., Urai, J.L., 2013. Clay-smear continuity and normal fault zone geometry – first results from excavated sandbox models. Journal of Structural Geology 57, 58-80.

Pei, Y., Paton, D.A., Knipe, R.J., Wu, K., 2015. A review of fault sealing behaviour and its evaluation in siliciclastic rocks. Earth-Science Reviews 150, 121–138.

Power, W.L., Tullis, T.E., Weeks, J.D., 1988. Roughness and wear during brittle faulting. Journal of Geophysical Research 93 (B12), 15268–15278.

Rawling, G.C., Goodwin, L.B., 2003. Cataclasis and particulate flow in faulted, poorly lithified sediments. Journal of Structural Geology 25, 317-331.

Rivenæs, J.C., Dart, C. 2002. Reservoir compartmentalisation by water-saturated faults – Is evaluation possible with today's tools? In: Koestler, A. G. & Hunsdale, R. (eds) Hydrocarbon Seal Quantification. Norwegian Petroleum Society, Special Publication 11, 173–186.

Robertson, E.C., 1983. Relationship of fault displacement to gouge and breccia thickness. American Institute of Mining Engineering Transactions 35, 1426–1432.

Rotevatn, A., Fossen, H., 2012. Soft faults and hard tips: magnitude-order displacement gradient variations controlled by strain softening versus hardening; complications for fault scaling. Journal of the Geological Society of London 169, 123-126, doi:10.1144/0016-76492011.108.

Sagy, A., Brodsky, E.E., Axen, G.J., 2007. Evolution of fault-surface roughness with slip. Geology 35, 283-286.

Sammis, C.G., King, G., Biegel, R., 1987. The kinematics of gouge deformation. Pure and Applied Geophysics 125, 777–812.

Schlische, R.W., Young, S.S., Ackermann, R.V., Gupta, A., 1996. Geometry and scaling relations of a population of very small rift-related normal faults. Geology 24, 683-686.

Scholz, C., 1987. Wear and gouge formation in brittle faulting. Geology 15, 493-495.

Seebeck, H., Nicol, A., Giba, M., Pettinga, J., Walsh, J., 2014. Geometry of the subducting Pacific plate since 20 Ma, Hikurangi margin, New Zealand. Journal of the Geological Society of London 171, 131-143. doi.org/10.1144/jgs2012-145.

Sibson, R.H., 1977. Fault rocks and fault mechanisms. Journal of the Geological Society of London 133, 191-231.

Sperrevik, S., Gillespie, P.A., Fisher, Q.J., Halvorsen, T., Knipe, R.J., 2002. Empirical estimation of fault rock properties. In: Koestler, A. G. & Hunsdale, R. (eds) Hydrocarbon Seal Quantification. Norwegian Petroleum Society, Special Publication 11, 109–125.

Van der Zee, W., Urai, J.L., 2005. Processes of normal fault evolution in a siliciclastic sequence: a case study from Miri, Sarawak, Malaysia. Journal of Structural Geology 27, 2281-2300.

Vrolijk, P.J., Urai, J.L., Kettermann, M., 2016. Clay smear: Review of mechanisms and applications. Journal of Structural Geology 86, 95-152.

Wallace, R.E., Morris, H.T., 1986. Charateristics of faults and shear zones in deep mines. Pure & Applied Geophysics 124(1/2), 105-25.

Walsh, J. J., Watterson, J., 1988. Analysis of the relationship between displacements and dimensions of faults. Journal of Structural Geology 10, 239-247.

Walsh, J. J., Watterson, J., Heath, A., Gillespie, P. A., Childs, C., 1998. Assessment of the effects of sub-seismic faults on bulk permeabilities of reservoir sequences. Geological Society, London, Special Publications 127(1), 99-114.

Watterson, J., Childs, C., Walsh, J.J., 1998. Widening of fault zones by erosion of asperities formed by bed-parallel slip. Geology 26, 71-74.

Wibberley, C.A.J., Yeilding, G., Di Toro, G., 2008. Recent advances in the understanding of fault zone internal structure: a review. In: C.A.J. Wibberley et al., eds. The Internal Structure of Fault Zones: Implications for Mechanical and Fluid Flow Properties. London: Geological Society Special Publications 299, 5-33.

Yielding, G., Freeman, B., Needham, D.T., 1997. Quantitative fault seal prediction. American Association of Petroleum Geologists Bulletin 81, 897–917.

Yielding, G., 2002. Shale Gouge Ratio - calibration by geohistory. In: Koester, A.G.H.R. (Ed.), Hydrocarbon Seal Quantification, NPF Special Publication, vol. 11. Elsevier, Amsterdam, pp. 1-15.

Yielding, G., Bretan, P., Freeman, B., 2010. Fault seal calibration – a brief review. In: Reservoir Compartmentalization (eds Jolley S.J, Fisher Q.J, Ainsworth R.B, Vrolijk P.J, Delise S). Geological Society of London Special Publication 347, 243-255.

Zhang, Y., Gartrell, A., Underschultz, J.R., Dewhurst, D., 2009. Numerical modelling of strain localisation and fluid flow during extensional fault reactivation: Implications for hydrocarbon preservation. Journal of Structural Geology 31(3), 315-327.

Figure Captions

Figure 1. Schematic diagrams showing current models for fault-rock developed by (a) sand-silt smear and (b) cataclasis. Dotted lines in lower diagrams define fault-zone boundaries which, for the purposes of this diagram, are parallel and produce fault zones of constant thickness, which is an oversimplification for most fault zones.

Figure 2. Maps and cross section showing the regional tectonic setting (a), geology of the northern Taranaki Basin and location of the study area (dot) on the west coast of New Zealand's North Island (b). Fault map in (b) for the base Miocene horizon. Cross section A-A' shows faults (steep black lines), Miocene to Recent strata (grey fill), Oligocene-Paleocene strata (white fill), Cretaceous strata (stipple) and Mesozoic basement (randomly oriented short lines). (c) Google Earth image showing the locations of Figures 3, 4, 5, 10, and 13.

Figure 3. Line drawings of small (a), medium (b) and larger (c) displacement faults within the Mount Messenger Formation showing the geometries of fault zones and locations of PSD samples (red filled circles). Dark grey polygons and white polygons represent siltstone and sandstone beds, respectively. Light grey polygons in (b) and (c) indicate fault zone location and geometry.

Figure 4. Outcrop photographs showing examples of fault rock from the MMF at Tongaporutu primarily generated by cataclasis of sandstone beds. (a) Cross-cutting deformation bands with displacements of <26 mm. (b) Light grey deformation bands that define a fault zone up to 40 mm wide and are associated with a dark grey discontinuous silt smear. (c) Light grey deformation bands within a fault zone up to 50 cm wide. Zone dominated by deformation bands is labelled DBZ, while fault gouge is labelled FG.

Figure 5 Outcrop photographs showing examples of faulted silt beds associated with silt smear (a & b lower cutoff) and no silt smear (b upper cutoff & c). All faults from the MMF. Inset in b) shows details of the silt smear geometry which is cross-cut by a small fault that locally influences the smear geometry.

Figure 6. Particle size distributions for sandstone (a) and siltstone (b) beds within the MMF. Red thick lines indicate the arithmetic mean curves for each rock type. Grain size boundaries for clay (≤2 µm), silt (2-63 µm) and sand (63-2000 µm) sized particles are indicated by the thin vertical dashed lines (International grain size scale ISO 14688-1:2002).

Figure 7. Displacement vs fault rock thickness plot. (a) Data for individual faults where the bars indicate the range of thicknesses observed along sample lines approximately parallel to fault dip over distances of 2-10m. (b) Same data as in (a) with the thicknesses for fault rock interpreted to have developed exclusively by cataclasis (red symbols) and silt smear (blue symbols) differentiated.

Figure 8. Thin section photo micrographs in cross-polarised light of deformation bands and associated particles of reduction size for sandstone host material. (b, c, d) Detailed photos of deformation bands with varying degrees of grain-size reduction. Red arrows indicate locations of trans-granular fractures and white arrows indicate rounded grains. The locations of (b, c, d) are shown by the red boxes in (a). Blue colour in photographs is epoxy used to maintain sample integrity during thin section preparation.

Figure 9. SEM backscatter images of (a) unfaulted sandstone (shear strain = 0), (b) fault rock from ~1.5 mm wide deformation band with 1.5 mm displacement in sandstone (i.e. shear strain = 1), and (c) fault rock from ~1-2 mm deformation band with 65 mm displacement in sandstone (i.e. shear strain = ~30-65).

Figure 10. Fault and bed geometries for intermediate-scale structure observed within a coastal cliff section (displacement ~1.4 m). Dark grey polygons indicate siltstone beds and silt smear, white polygons sandstone beds and light grey sandstone within fault zone (these sandstone areas may be undeformed or comprise deformation bands). PSDs and their locations are also shown by the numbered red filled circles and the arrows (sample number is shown in brackets on the PSD). PSD fill colours match those of the fault cross section (i.e. dark grey is siltstone/silt, white sandstone and light grey faulted sandstone within the fault zone).

Figure 11. PSDs from sandstone protolith and deformation bands (a-h) and for siltstone protolith and silt smear (i-l). Each graph shows the PSD for the protolith material (red line) and the resultant fault rock (black line). Fault displacements (Displ.) and fault-rock thickness (FRT) are presented for each PSD. DB=deformation band and Sst= sandstone. In f) PSD measurements for samples comprising 1 deformation and 12 deformation bands are presented; the later has slightly higher sandstone mode which may be due to the presence of undeformed grains between bands.

Figure 12. PSDs for fault gouge with displacements larger than the thickness of sandstone beds (e.g., >1.5 m) and unknown protolith. Based on visual inspection the gouge protolith is inferred by comparing its PSD with those of unfaulted sandstone and siltstone beds. Fault gouge with a PSD comprising a sandstone mode at ~90-110 µm is inferred to be mainly derived from a sandstone protolith (a). Alternatively, fault gouge comprising a PSD which is comparable to that of siltstone beds is inferred to be derived from siltstone protolith (b). Red lines show average sandstone and siltstone PSDs and the grey lines average cataclastic and silt smear PSDs for all data.

Figure 13. Relationships between fault-rock thickness, displacement and bed lithology for a small fault (mean displacement ~7.7 cm) in a sandstone dominated sequence. (a) Cross section showing fault zone, beds and locations of PSD locations. Cross section rotated approximately 70º clockwise. (b) Graph of fault-rock thickness and displacement versus distance along the fault trace. Locations of faulted siltstone beds are indicated by grey polygons in the graph.

Highlights

Nicol and Childs - Cataclasis and shale smear on normal faults in a weakly lithified multilayer

- Fault rock is produced by a combination of sandstone cataclasis and shale smear.
- Cataclasis is initially rapid, continues with increasing displacement and accounts for more than 50% of fault rock.
- Shale smear occurs without significant particle-size reduction via intergrain slip and micro-faulting.
- Variations in fault-rock thickness and associated cataclasis have the potential to modify the hydraulic properties of faults and may need to be accounted for in fluid-flow models.